EPJ Web of Conferences **340**, 01004 (2025) https://doi.org/10.1051/epjconf/202534001004
Powders & Grains 2025

Stress transmission and fabric states in granular materials

Farhang Radjai[1,*], *Duc Chung* Vu[2], and *Lhassan* Amarsid[3]

[1]LMGC, University of Montpellier, CNRS, 163 rue Auguste Broussonnet, 34090 Montpellier, France
[2]Hanoi University of Civil Engineering, Faculty of Hydraulic Engineering, 55 Giai Phong street, Hanoi, Vietnam
[3]CEA, DES, IRESNE, DEC, Cadarache F 13108 Saint Paul lez Durance, France.

Abstract. Force transmission in granular materials involves two key aspects that have generally been treated separately: (1) the broad probability density function of force magnitudes, and (2) the anisotropic distribution of contact orientations and the forces they transmit. In this paper, we first analyze the origins of the exponential distribution of strong forces and the non-exponential behavior observed in the weak-force range. We show that the exponential tail arises naturally from the statistical independence of contact forces acting on each particle, a consequence of the inherent disorder in granular packings. We then introduce a self-consistent force model for isotropic systems with a single free parameter that accounts for the non-exponential behavior of weak forces. We extend this model to account for both fabric and force anisotropies. We show that the resulting anisotropic force distribution successfully captures the bimodal nature of force transmission, as well as the dependence of the force statistics on the underlying fabric and force anisotropies.

1 Introduction

The inhomogeneous distribution of contact forces is a well-established feature of granular materials, as evidenced by experimental observations and discrete element simulations [1–4]. The probability density function (PDF) of the normal components or magnitudes of contact forces typically exhibits an exponential decay at large forces and a nonzero probability density for forces approaching zero. Simulations further reveal that in sheared granular assemblies, the force network organizes into distinct weak and strong sub-networks. The strong network predominantly sustains the shear strength, while the weak forces primarily contribute to prop strong force chains [5]. Extensive studies have demonstrated that the exponential tail of the strong force distribution is a robust feature across both two- and three-dimensional systems. By contrast, the behavior of weak forces is more sensitive to the packing state, which is influenced by parameters such as particle size distribution, particle shape, and the amount of shearing [6–9]. In isotropic packings, the force distribution displays a relatively small peak below the mean force. However, under shear, this peak vanishes, and the distribution of weak forces evolves toward a decreasing power-law form [4, 10]. Furthermore, the application of shear induces both fabric and force anisotropies, aspects that have often been studied in connection with shear strength but independently of force distributions [11, 12].

Force balance conditions, granular disorder, and steric exclusions are the primary origins of the characteristic features observed in force distributions within granular materials. These fundamental features are minimally captured by the q-model [1, 13], in which forces “propagate" from one layer of particles to the next along contacts arranged on a regular network. In this model, force balance is ensured through local force conservation, while disorder is introduced via stochastic redistribution of forces between layers. The q-model predicts an asymptotically exponential distribution of contact forces. Subsequent developments have focused on the density of states within a first-shell approximation, considering a particle and its immediate contacting neighbors, and analyzing the local constraints imposed by force balance [14]. Sampling force configurations within such local structures yields PDFs that closely match those obtained from discrete element simulations. Alternative semi-analytical approaches have also been explored to better fit the force PDFs observed in isotropic dense packings. In particular, it was shown that a linear combination of several functional forms can accurately reproduce the empirical distributions in the isotropic case [15].

In this paper, we combine theoretical analysis and numerical simulations to address two central questions: (1) What is the nature of granular disorder, and how can steric exclusions and force balance be incorporated into a self-consistent model that accounts for the exponential distribution of strong forces? (2) How can fabric and force anisotropies be integrated into a general framework for force distributions? To this end, we introduce a self-consistent extension of the q-model, implying that the interplay between vectorial force balance and granular disorder naturally leads to an exponential distribution of forces. Furthermore, we revisit a force model based on population balance, incorporating a single free parameter that reflects the packing state, and use it to construct the joint

*e-mail: franck.radjai@umontpellier.fr

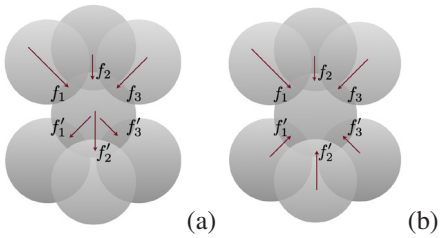

Figure 1. (a) Representation of a particle and the downward incoming and outgoing forces in the q-model. (b) Downward and upward forces in a symmetric representation of forces.

PDF of contact forces and orientations. Our results show that the joint PDF successfully captures the broadening of the force distribution, derived as a marginal distribution of the joint PDF, under increasing anisotropy. Furthermore, it predicts the organization of contact forces into weak and strong sub-networks.

2 Self-consistent force model

2.1 The q-model

The q-model describes the diffusive "propagation" of forces along a given direction z inside a granular particle assembly [1, 13]. In this model, the force is treated as a scalar quantity, and the z-axis plays the role of a temporal coordinate. As illustrated in Fig. 1(a), each particle receives contact forces from particles located above and redistributes them to particles below. While the number of contact neighbors may vary in general, for the sake of clarity one may consider that each particle interacts with three neighbors on both its upper and lower sides. The total incoming force on a particle is denoted by $w = \sum_i f_i$, where f_i are the individual forces transmitted from above. This total force is redistributed downward according to a random process: $f'_i = q_i w$, where the q_i are independent random variables uniformly distributed in the interval $[0, 1]$, subject to the constraint $\sum_i q_i = 1$. This constraint ensures force conservation during the downward propagation, a condition that is equivalent to maintaining force balance at the level of individual particles. Although the forces applied at the top layer of the system may be arbitrary, the repeated application of this process along the z-direction leads asymptotically to an exponential PDF of forces: $P_f(f) = \beta e^{-\beta f}$. Since the mean force $\langle f \rangle = 1/\beta$, the distribution of forces normalized by $\langle f \rangle$ implies $\beta = 1$. The exponential distribution of forces leads to a Gamma distribution of w: $P_w(w) = (\beta^3/2) w^2 e^{-\beta w}$.

2.2 A self-consistent approach

The primary limitation of the q-model lies in its inherently diffusive character, which stems from the unidirectional propagation of forces. This aspect violates the mechanical up-down symmetry expected in static granular assemblies and leads to an exponential force distribution only as an asymptotic result of multiple layers of forward propagation. To restore this fundamental symmetry, the model must treat the forces transmitted from above and below in a symmetric manner. This condition is naturally satisfied by the local force balance equation:

$$\sum_i f_i = \sum_i f'_i, \tag{1}$$

where the sign convention is defined as shown in Fig. 1(b).

To enforce symmetry in the probability distributions of forces, we consider $P_3(f_1, f_2, f_3)$ and $P'_3(f'_1, f'_2, f'_3)$ as the joint PDFs of the contact forces acting on the upper and lower hemispheres of a particle, respectively. The forces f_i are directed downward, while the f'_i are directed upward. Enforcing up-down symmetry thus leads to the condition:

$$P_3(f_1, f_2, f_3) = P'_3(f'_1, f'_2, f'_3). \tag{2}$$

In this formulation, it is no longer appropriate to relate f_i and f'_i through random partitioning coefficients q_i, as is done in the q-model. Instead, the force configurations on the upper and lower sides of the particle are intrinsically related through Eq. (2). The only additional requirement is the inclusion of granular disorder.

Given that the forces f_i and f'_i are scalar quantities, a natural and minimal assumption to incorporate disorder is to treat these forces as independent, identically distributed (i.i.d.) random variables. This implies that

$$\begin{aligned} P_3(f_1, f_2, f_3) &= P_f(f_1) P_f(f_2) P_f(f_3), \\ P'_3(f'_1, f'_2, f'_3) &= P_f(f'_1) P_f(f'_2) P_f(f'_3), \end{aligned} \tag{3}$$

where $P_f(f)$ denotes the single-force probability density function.

Substituting Eq.(3) into Eq.(2) and taking the logarithm of both sides yields the relation:

$$\sum_i \ln P_f(f_i) = \sum_i \ln P_f(f'_i). \tag{4}$$

This equation implies that $\ln P_f(f)$ is an additive invariant under the force redistribution process, in the same sense that Eq. (1) expresses the additive invariance of the forces. Since the only scalar additive physical invariants in this context are the force itself and a constant that can be added to all forces, it follows that $\ln P_f(f)$ must be a linear combination of these physical invariants:

$$\ln P_f(f) = a + bf, \tag{5}$$

which implies an exponential form for the force distribution:

$$P_f(f) = \beta e^{-\beta f}. \tag{6}$$

This approach is similar to the derivation of the Maxwell-Boltzmann distribution in kinetic theory, where the local distribution of molecular velocities implies five conserved quantities and the assumption of molecular chaos [16]. In the granular context, the assumption of statistical independence of the forces—formalized in Eq. (3)—plays a role analogous to that of molecular chaos. This self-consistent approach demonstrates that the exponential force distribution observed in the q-model on a regular lattice is not a consequence of a specific distribution

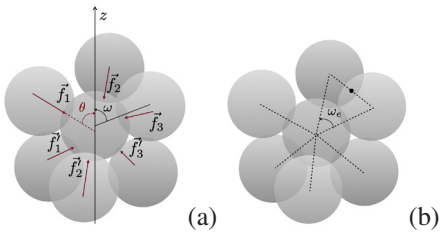

Figure 2. (a) A particle with random angular application points of force vectors exerted by contact neighbors. (b) Exclusion angle ω_e between neighboring particles.

of the q variables. Rather, it emerges from the statistical independence of the contact forces due to disorder. Indeed, prior studies have confirmed that the exponential form of $P_f(f)$ in the q-model is robust and remains unchanged for different distributions of the q variables [1].

2.3 A vectorial model

The self-consistent scalar model does not explicitly account for the full randomness of contact forces, as it is defined on a regular lattice of particles with fixed geometry. In contrast, the full vectorial problem, illustrated in Fig. 2(a), involves both the randomness in the contact positions at which forces are exerted by neighboring particles and the variability in the force orientations up to a limit allowed by solid friction between particles. The contact forces, exerted by neighboring particles in contact with the central particle, satisfy the vectorial force balance condition:

$$\sum_i \vec{f}_i = \sum_i \vec{f}'_i, \tag{7}$$

where $\vec{f}_i$ and $\vec{f}'_i$ denote the force vectors acting on the particle from above and below, respectively. Moreover, the angular positions of contact neighbors are not arbitrary but are subject to steric constraints due to geometric exclusion between adjacent particles. This constraint is expressed by:

$$\omega_{ij} \leq \omega_e, \tag{8}$$

where ω_{ij} is the angular separation between the branch vectors connecting the center of the reference particle to the centers of two adjacent contacting neighbors i and j, as shown in Fig. 2(b).

The presence of these angular hindrances not only limits the number of potential contact neighbors but also induces a degree of correlation between adjacent contact forces. Let $f_{zi} = f_i \cos\theta_i$ and $f_{zj} = f_j \cos\theta_j$ be the vertical components of the forces exerted by two adjacent particles i and j on the reference particle, where θ_i and θ_j represent the polar angles of the force vectors $\vec{f}_i$ and $\vec{f}_j$ with respect to the z-axis. In the case of frictionless particles, these force orientations θ_i and θ_j coincide with the angular positions ω_i and ω_j of the contacting particles. Given the steric exclusion condition $|\omega_{ij}| \geq \omega_e$, the vertical components f_{zi} and f_{zj} cannot assume arbitrary values, as their directions are geometrically constrained.

For frictional particles, however, the force orientations θ_i and θ_j may deviate from the geometrical contact directions ω_i and ω_j due to the finite static friction coefficient μ_s. In this case, the force vector can deviate from the branch vector within the Coulomb friction cone. The steric exclusion angle ω_e is equal to $\pi/3$ for spherical particles of identical size. When the static friction coefficient satisfies $\mu_s \geq \tan(\pi/6) \simeq 0.577$, two adjacent contact forces can, in principle, become parallel despite geometric exclusion. Therefore, as the friction coefficient increases, geometry imposes less stringent constraints on force orientation.

In the presence of steric constraints, we may treat the magnitudes $f = \sqrt{f_x^2 + f_y^2 + f_z^2}$ of the contact force vectors acting on a particle as independent random variables. In fact, the proper disorder of a granular packing lies in the high variability of the particle environments in terms of contact positions and values of forces. The interferences between these environments results in relative randomness of force magnitudes. Despite this randomness in force magnitudes, their orientations are subject to strong geometric correlations. At the level of individual particles, the number of accessible contact configurations is therefore highly constrained. Although contact orientations around a given particle are strongly correlated due to steric hindrance, they remain broadly distributed and effectively uncorrelated at larger scales. However, the length scale over which this transition from local order to global disorder occurs is not immediately apparent.

We assume that the force vectors are fully random identically distributed and independent variables despite steric exclusions. Their joint probability densities P_3 and P'_3 then factorize into products of single-vector distributions P_f and P'_f:

$$\begin{aligned} P_3(\vec{f}_1, \vec{f}_2, \vec{f}_3) &= P_f(\vec{f}_1) P_f(\vec{f}_2) P_f(\vec{f}_3), \\ P'_3(\vec{f}'_1, \vec{f}'_2, \vec{f}'_3) &= P_f(\vec{f}'_1) P_f(\vec{f}'_2) P_f(\vec{f}'_3). \end{aligned} \tag{9}$$

We again assume up-down symmetry, implying

$$\sum_i \ln P_f(\vec{f}_i) = \sum_i \ln P_f(\vec{f}'_i). \tag{10}$$

Given that this relation must hold for all sets of vectors satisfying the force balance constraint (7), the logarithm of the single-vector probability density must be a linear function of $\vec{f}$:

$$\ln P_f(\vec{f}) = \vec{b} \cdot \vec{f}, \tag{11}$$

implying that

$$P_f(\vec{f}) = C e^{-|\vec{b} \cdot \vec{f}|}, \tag{12}$$

with $C = b_1 b_2 b_3$ enforcing normalization, $b_i \geq 0$, and $\vec{f} \in \mathbb{R}^3_+$. This formulation can accommodate anisotropic textures in which the mean force depends on direction. In the case of an isotropic packing with rotational symmetry, we have $b_1 = b_2 = b_3 = b$, so that

$$P_f(f_x, f_y, f_z) = b^3 e^{-b(f_x + f_y + f_z)}. \tag{13}$$

This equation means that the force PDF is the product of three independent exponential functions with $f_i \geq 0$.

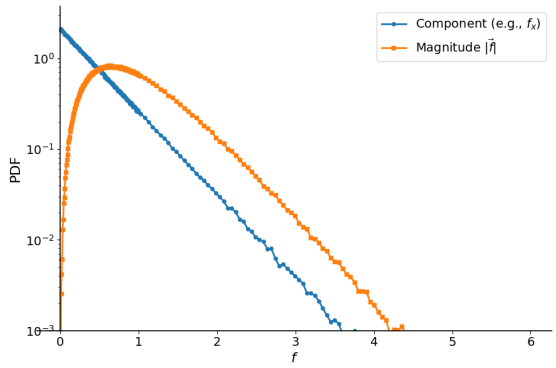

Figure 3. PDF of force magnitudes f calculated numerically from that of its components, assumed to be an exponential function.

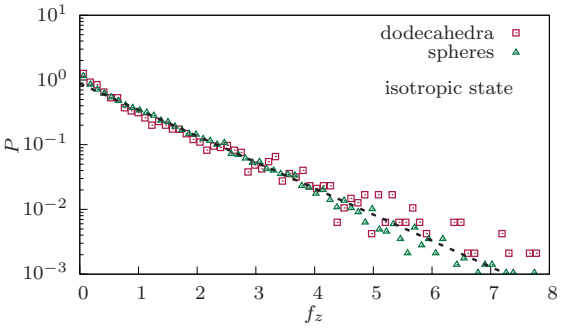

Figure 4. The probability density functions of the z components of contact forces in two simulated dense isotropic packings, composed respectively of spherical and dodecahedral particles. For comparison, a dashed line is plotted to represent a normalized exponential function.

In the next step, the objective is to determine the force distribution P_f of force magnitudes $f = \sqrt{f_x^2 + f_y^2 + f_z^2}$ from the known exponential distribution P_{f_i}. Let us define $r_i = f_i^2$ with each f_i governed by an exponential PDF. The PDF of r_i can be derived using transformation of variables:

$$P_{r_i}(r_i) = \frac{1}{2\sqrt{r_i}} b e^{-b\sqrt{r_i}}. \tag{14}$$

Since $f^2 = r_1 + r_2 + r_3$, f^2 is the sum of three independent ariables r_i, each with the above PDF. The distribution of f then follows by

$$P_f(f) = \frac{d}{df} P(f^2 < r) = 2f P_{f^2}(f^2). \tag{15}$$

Unfortunately, there is no closed-form expression for this sum. But we can sample and plot it. Figure 3 shows the PDF of f numerically calculated from that of its components f_z, which is assumed to be a normalized exponential function. The force magnitudes above the mean fall off exponentially and a peak occurs for f slightly below the mean force, but, in contrast to common observation, the PDF vanishes with vanishing force ($P_f(f) \to 0$ as $f \to 0$), as also expected from equation (17).

This discrepancy is a consequence of the higher density of P_{f_i} at low values of f_i. Figure 4 presents the PDFs of f_z in two frictionless packings, each consisting of 8000 particles—either spheres or regular dodecahedra—prepared by isotropic compaction. The simulations were performed using the discrete element method (DEM) under fully periodic boundary conditions. A detailed description of the simulations are given in Ref. [19]. Since weak forces are sensitive to the numerical precision, the compaction process is stopped only when all contacts and forces are stable in time and no force fluctuations occur across the system. This ensures that all particles have reached static equilibrium with a high precision. The PDFs coincide within statistical precision and are heavier than exponential as $f_z \to 0$. This heavier density is therefore the origin of the nonvanishing PDF P_f of force magnitudes at $f \to 0$.

The higher density of P_{f_z} in the range $f_z \to 0$ indicates that weak force components are not fully independent. We calculated the Pearson correlation coefficient of f_z for forces acting on the upper and lower hemispheres of particles according to the z axis in the two simulated samples mentioned previously. The correlation coefficient was 0.1 for all forces. When considering separately the forces f_z below (weak) and above (large) $0.012\langle f_z\rangle$, the correlation coefficient was found to be -0.28 for weak-weak pairs, -0.05 for large-large pairs, and 0.008 for weak-large pairs. The low values of the coefficient for the large-large and weak-large pairs is consistent with the model assumptions and thus the exponential PDF of strong forces. Note also that weak values of f_z are due to either a weak force magnitude or a high value of the projection angle (close to $\pi/2$). The higher density of P_{f_z} at small values of f_z. Steric exclusions lead therefore to correlations only among weak pairs of forces acting on a particle. Two weak components separated by an angle of exclusion of $\pi/3$ can be respectively a large force with a high projection angle and a small force acting at an angular distance of $\pi/3$ from the first one. The higher correlation coefficient of weak pairs indicates that strong forces tend to be neighbors to weak forces.

Despite its simplicity, this self-consistent vectorial model effectively captures the nearly exponential distribution of strong forces, along with the relatively minor influence of steric exclusions. However, it fails to account for the behavior of weak forces, which appears to result from long-range correlations rather than steric constraints alone. It is also worth noting that, although we specifically considered a configuration with six contacts—three on each hemisphere—the core arguments of the model remain generally applicable. The only notable exception arises when there is a single contact on one hemisphere, a rare and atypical case. Note also that we consider here only the magnitudes of forces or their components along different directions. However, by extending the same assumptions of statistical independence and vectorial balance to force moments, one arrives at exponential distributions of the normal and tangential (frictional) components of the contact forces.

3 Anisotropic force distributions

In the formulation of the self-consistent vectorial model, no specific assumption was made regarding the orientations of forces or contacts. However, a privileged direction z was introduced to distinguish between the two hemispheres of the reference particle. In the case of an isotropic contact network, we assume that the PDF is invariant under the choice of this reference direction. In contrast, sheared granular materials exhibit anisotropic microstructure, characterized by an accumulation of contacts along the compression direction and a depletion along the extension direction. Moreover, the forces transmitted through the contact depend on the orientations of their normals or brach vector orientations.

Anisotropic force distributions have been proposed by Kruyt [17] in 2D, and were used to predict theoretically the properties of the weak and strong contact networks. In what follows, we construct an anisotropic force distribution in 3D under boundary conditions that are invariant under rotations about a fixed axis. In this setting, the force distributions are invariant by rotation around the same axis and both fabric and force anisotropies can be expressed solely as functions of the polar angle θ with the axis. The distribution is built upon a base force model for the magnitudes of forces.

3.1 Base model

The base model described here provides a simple analytical expression for the PDF of force magnitudes f, capturing both the exponential decay at large forces and the nontrivial behavior observed at small forces. In contrast to the model presented in the previous section—which relied on a local perspective based on force balance at the particle level—the present model adopts a global viewpoint, grounded in a population balance argument for the distribution of forces.

We consider a hierarchy of forces ranging from zero to infinity. When forces are normalized by the mean force $\langle f \rangle$, which is proportional to the confining pressure via the relation $p = n_c \langle \ell f \rangle$ (where n_c denotes the contact number density and ℓ the branch vector length), the deviation of their population from a uniform distribution results from two competing processes: (1) the splitting of large forces into smaller ones, and (2) the combination of small forces into larger ones. Consequently, the frequency with which a force magnitude f is realized depends on the number of forces both larger and smaller than f. Since these processes obey vector algebra, they do not imply the loss of the larger or smaller forces that give rise to f. This type of reasoning is reminiscent of statistical models in population dynamics, which often describe population changes using local exchange rules between neighboring sites on a lattice [18]. Although no time evolution is considered in the present context, we aim to formulate a rule that reflects the essence of the split/combine process and governs the balance between the populations associated with different force levels.

The simplest version of such a model is based on the assumption that the probability density function $P_f(f)$ of force magnitude f is proportional to the probability density $G(f) = \int_f^\infty P_f(x)\,dx$ of forces exceeding f, scaled by a factor b that quantifies the relative weight of the splitting process [10]. The remaining proportion of forces, $1 - bG(f)$, is then interpreted as the contribution of lower forces that may combine to produce a force of magnitude f or play the role of weak forces probing stronger forces. Accordingly, $P_f(f)$ is also assumed to be proportional to $1 - bG(f)$. These two assumptions jointly lead to the following simple integral-differential equation governing the form of $P_f(f)$:

$$P_f(f) = abG(f)[1 - bG(f)], \tag{16}$$

where a is the normalization factor, $G(f) = \int_f^\infty P_f(x)\,dx$, $\int_0^\infty P_f(f)\,df = 1$, and $\int_0^\infty f P_f(f)\,df = 1$.

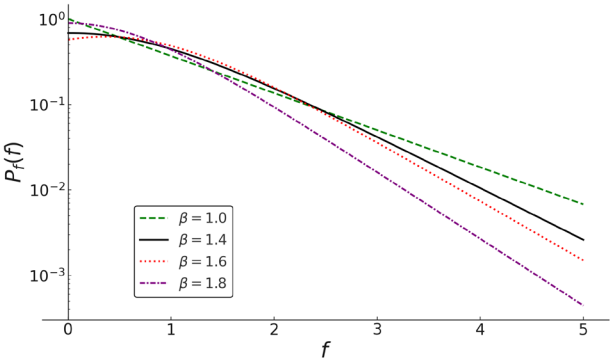

Figure 5. Force PDF for several values of decay rate β according to equation (17).

Equation (16) can be solved straightforwardly, yielding the following analytical expression for the force distribution:

$$P_f(f) = \beta(1+\gamma)\frac{\gamma e^{\beta f}}{(1+\gamma e^{\beta f})^2}, \tag{17}$$

where $\beta = ab$ and $\gamma = 1/b - 1$. In this form, $P_f(f)$ is a normalized PDF governed by two parameters, β and γ. However, enforcing the constraint $\langle f \rangle = 1$ leads to a functional relation between the two parameters:

$$\beta = (1+\gamma)\ln\left(\frac{1+\gamma}{\gamma}\right). \tag{18}$$

Figure 5 displays the resulting distribution $P_f(f)$ for four values of β. These curves exhibit all the characteristic features observed in empirical force distributions. In particular, the value of the PDF at zero force is given by $P_f(0) = \gamma \ln[(1+\gamma)/\gamma]$, which increases monotonically with γ. For $\gamma \leq 1$, the distribution exhibits a peak located at $f = -\ln\gamma/\{(1+\gamma)\ln[(1+\gamma)/\gamma]\}$ which lies at $f = 0$ when $\gamma = 1$, and shifts to higher values of f as γ decreases. Furthermore, in the limit of large forces, the distribution asymptotically approaches an exponential form.

Figure 6(a) presents the PDFs of contact forces in the two samples previously mentioned. The data are well fitted by the analytical expression given in equation (17) by

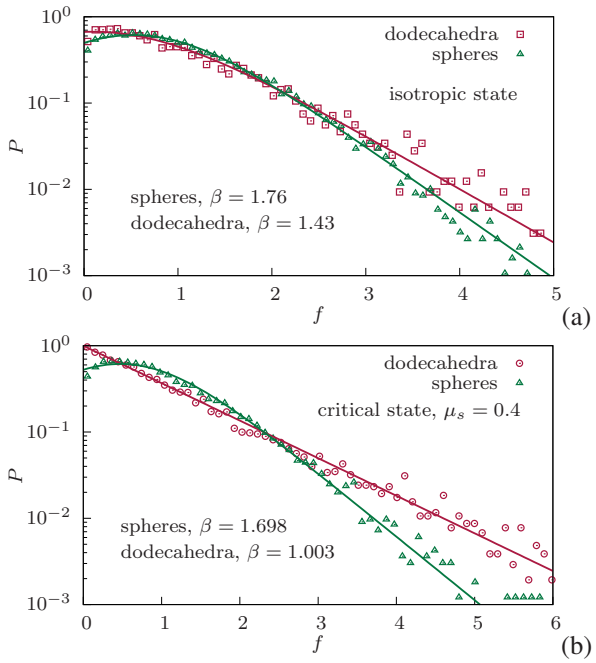

Figure 6. The probability density functions of contact forces in two simulated packings, composed respectively of spherical and dodecahedral particles. The solid lines represent fits based on the analytical expression given in equation (17), with specified values of the decay rate β. (a) isotropic frictionless packings, (b) sheared packings with friction coefficient $\mu_s = 0.4$.

adjusting the single parameter β. The broader distribution observed for dodecahedral particles reflects the greater inhomogeneity of force transmission, which arises from the presence of face-face contacts in the packing.

In general, since the functional form of the PDF is governed by a single free parameter γ or β, the influence of mechanical factors—such as interparticle friction or force anisotropy—should manifest primarily through variations in this parameter. For instance, shearing often leads to a lower coordination number and higher anisotropy, which in turn results in a more heterogeneous force network. This trend is illustrated in Fig.6(b), where force distributions are shown for the same spherical and dodecahedral packings as in Fig.6(a), but now subjected to shear under a nonzero interparticle friction coefficient μ_s. For both particle shapes, the fitted value of β is lower in the sheared state than in the initially compacted isotropic state.

3.2 Anisotropic force distribution

Let us now consider the PDF of forces given by equation (17). We would like to make this distribution depend on the orientations of contacts or branch vectors joining particle centers. For the sake of simplicity, we assume that the material is invariant by rotation around the z axis, so that the distribution of orientations depends only on the polar angle θ with the z-axis. We may approximate the distribution of orientations by a truncated spherical harmonics function

$$P_\theta(\theta) = \frac{1}{4\pi}\Big(1 + a_c(3\cos^2\theta - 1)\Big), \tag{19}$$

where a_c is the fabric anisotropy. We also assume that the force distribution is anisotropic and the directional average force is given by

$$\langle f\rangle_\theta = 1 + a_f(3\cos^2\theta - 1), \tag{20}$$

where a_f is the force anisotropy without distinguishing between its normal and tangential components.

To construct the joint probability density function $P(f,\theta)$, we use the given components: (1) normalized force marginal distribution $P_f(f)$, (2) contact orientation marginal $P_\theta(\theta)$, and (3) angular dependence of the mean force $\langle f\rangle_\theta$ Therefore, the joint PDF $P(f,\theta)$ must be such that

1. $P(f,\theta) = P(f|\theta)\,P_\theta(\theta)$
2. The conditional PDF $P(f|\theta)$ has mean $\langle f\rangle_\theta = 1 + a_f(3\cos^2\theta - 1)$
3. The functional form of $P(f|\theta)$ is identical to $P_f(f)$, but rescaled so that its mean is $\langle f\rangle_\theta$ rather than 1.

We first define a scaled version of P_f such that the mean is $h(\theta) = \langle f\rangle_\theta$. This is done by a change of variable:

$$P(f|\theta) = \frac{1}{h(\theta)} P_f\left(\frac{f}{h(\theta)}\right). \tag{21}$$

This ensures normalization $\int_0^\infty P(f|\theta)df = 1$ and the mean $\int_0^\infty fP(f|\theta)df = h(\theta)$. But it does not ensure that the average force is 1. The average force is given by

$$\langle f\rangle = \int P_\theta(\theta)h(\theta)\sin\theta\, d\theta d\phi = 1 + \frac{4}{5}a_c a_f. \tag{22}$$

To enforce $\langle f\rangle = 1$, we rescale all forces by the global mean so that the rescaled mean is

$$\tilde{h}(\theta) = \frac{1 + a_f(3\cos^2\theta - 1)}{1 + \frac{4}{5}a_c a_f} \tag{23}$$

This leads to the joint distribution

$$\begin{aligned} P(f,\theta) &= P(f|\theta)P_\theta(\theta) \\ &= \tfrac{1}{\tilde{h}(\theta)} P_f\left(\tfrac{f}{\tilde{h}(\theta)}\right) \times \tfrac{1}{4\pi}\Big(1 + a_c(3\cos^2\theta - 1)\Big) \end{aligned} \tag{24}$$

Expanding explicitly, we have

$$P(f,\theta) = \frac{\beta(1+\gamma)}{4\pi\tilde{h}(\theta)}\Big(1 + a_c(3\cos^2\theta - 1)\Big)\frac{\gamma e^{\beta f/\tilde{h}(\theta)}}{\Big(1 + \gamma e^{\beta f/\tilde{h}(\theta)}\Big)^2}. \tag{25}$$

With this expression we recover $P_\theta(\theta)$ from integration over f and $P_f(f)$ is recovered for $a_f = 0$ and integrating over θ. In the next section, we consider several predictions of this joint PDF.

3.3 Effective force distributions

From the joint PDF $P(f,\theta)$ given by (25), we can derive an effective force distribution for anisotropic systems by integrating over θ:

$$P_f^{\text{eff}}(f) = 2\pi\int_0^\pi P(f,\theta)\,\sin\theta\, d\theta. \tag{26}$$

Since there is no simple analytical form of this integral, we plot in Fig. 7 the effective force distributions obtained by means of numerical integration for $\beta = 1.4$ and several values of a_c and a_f. The distributions become broader with increasing a_f but a_c has practically no effect. Indeed, at large f, the dominant behavior of the effective force distribution is

$$P_f^{\text{eff}}(f) \sim \exp\left(-\beta f/\tilde{h}_{\max}\right), \tag{27}$$

where $\tilde{h}_{\max} = \max_\theta\{\tilde{h}(\theta)\} = (1 + 2a_f)/(1 + 0.8a_c a_f)$. This tells us that the tail decay rate is set by $\tilde{h}_{\max}$, i.e., how large the local mean force gets. The lower bound of the effective decay rate is therefore given by $\lambda_{min} = \beta(1 + 0.8a_c a_f)/(1 + 2a_f)$. The contribution of a_c in this expression is overshadowed by that of a_f. The parameter a_c appears mainly in the angular distribution. It weights different orientations — giving more or less weight to regions of high/low $h(\theta)$. But it does not have strong influence on the value of $\tilde{h}(\theta)$ itself.

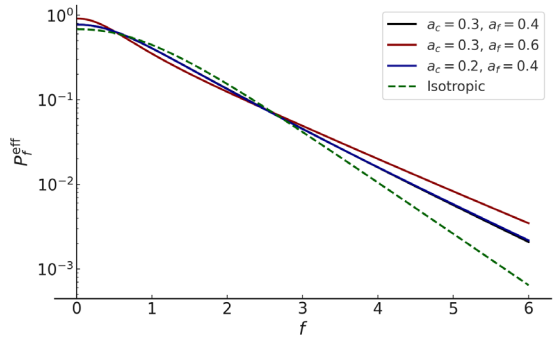

Figure 7. The effective PDF of contact forces in an anisotropic granular material as predicted by the joint PDF $P(f, \theta)$ given by equation (25) for $\beta = 1.4$ and several values of the fabric anisotropy a_c and force anisotropy a_f.

The decrease of β for spherical and dodecahedral particle packings in the numerical results displayed in Fig. 6(b) as compared to Fig.6(a) is in agreement with this estimate. We have $a_f = a_c \simeq 0$ in the isotropic packings with $\beta \simeq 1.43$ for dodecahedra. In the critical state, we have $a_f \simeq 0.4$ and $a_c \simeq 0.35$, which lead to $\lambda_{min} \simeq 0.88$, a value which is slightly below $\beta \simeq 1$ for dodecahedra in Fig. 6(b). For spherical particles, the numerical value of decay rate is above the predicted lower bound.

3.4 Predicting bimodal force distribution

Another interesting prediction of the anisotropic force PDF concerns the partial fabric anisotropy $a_{c\xi}$ and force anisotropy $a_{f\xi}$ associated with the subset of contact forces restricted to values below a threshold $\xi\langle f\rangle = \xi$. The partial fabric anisotropy $a_{c\xi}$ can be computed from its definition based on the spherical harmonics expansion (19):

$$a_{c\xi} = \frac{5}{4}\left(3\langle\cos^2(\theta)\rangle_\xi - 1\right), \tag{28}$$

where the average $\langle\cdots\rangle_\xi$ is taken over all contacts for which $f < \xi$. The partial force anisotropy $a_{f\xi}$ is extracted by fitting the directional average force $\langle f\rangle_\theta$ over the ξ-network to

$$\langle f\rangle_\theta^\xi \approx A + a_{f\xi}(3\cos^2\theta - 1), \tag{29}$$

where A is a constant offset.

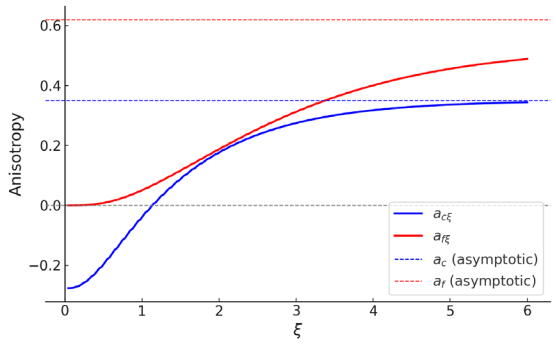

Figure 8. The partial anisotropies $a_{c\xi}$ and $a_{f\xi}$ of the ξ-network extracted from the anisotropic force PDF as a function of the force threshold ξ for $\beta = 1.43$, $a_c = 0.35$, and $a_f = 0.62$.

Figure 8 displays the two partial anisotropies as a function of ξ for $\beta = 1.43$, $a_c = 0.35$, and $a_f = 0.62$. We observe that $a_{c\xi}$ increases from an initially negative value, vanishes at $\xi \simeq 1$, and continues to increase with positive values, converging to its full-network value a_c as $\xi \to \infty$. The negative values of $a_{c\xi}$ indicate that the orientations of contacts carrying forces $f < 1$ are predominantly aligned in directions perpendicular to the z-axis. In contrast, for forces $f > 1$, $a_{c\xi}$ becomes positive, signifying that the corresponding contact orientations are aligned along the z-axis. These opposite signs of the anisotropies corroborate the bimodal nature of the force network, as previously revealed by DEM simulations in both 2D and 3D systems [4, 5]. In these studies, weak and strong forces were defined as those below and above the mean force, respectively. Their contrasting anisotropies support the intuitive picture in which strong force chains aligned with the compression direction are stabilized by laterally oriented weak forces. The transition between these two subnetworks occurs around $f \simeq 1$, where the total fabric anisotropy $a_{c\xi}(\xi = 1)$ of the weak network is approximately zero.

In contrast to $a_{c\xi}$, the partial force anisotropy $a_{f\xi}$ remains strictly positive across all values of ξ, but exhibits a slow, sigmoidal increase from zero toward its asymptotic value. The small magnitude of $a_{f\xi}$ within the weak force network, combined with the observation that $a_{c\xi}(\xi = 1) \simeq 0$, indicates that the weak network is approximately isotropic. This suggests that the global anisotropies a_c and a_f arise almost entirely from the strong force network, which carries forces above the mean. A notable feature in Figure 8 is the slow convergence of $a_{f\xi}$ to its asymptotic value. This behavior stems from the exponential decay of the force distribution $P_f(f)$ and the fact that the angular modulation of the average force becomes more pronounced at large force magnitudes. Therefore, the directional dependence of $\langle f\rangle_\theta$ sharpens as f increases, causing high-force contacts to contribute disproportionately to the overall force anisotropy.

Finally, it is also possible to evaluate $a_{c\xi}$ analytically in the limit $\xi \to 0$. A first-order analytical approximation, expanded to include linear and quadratic terms in the anisotropy parameters, yields:

$$a_{c\xi}\big|_{\xi\to 0} \approx a_c - a_f - \tfrac{4}{7} a_c a_f. \tag{30}$$

The third term on the right-hand side is of second order relative to the leading contributions. This approximation is in excellent agreement with the numerical result (≈ -0.276) shown in Fig. 8 for the parameters $a_c = 0.35$ and $a_f = 0.62$. It confirms that the negative anisotropy observed in the weak-force subnetwork is a direct consequence of the condition $a_c < a_f$, as also pointed out in the 2D case by Kruyt [17]. Our simulations (not shown here) reveal that this condition is not universally valid: in highly frictional packings subjected to shear, the weak network may instead align with the compression axis, resulting in a positive $a_{c\xi}$ even at small ξ.

4 Conclusions

In this work, we examined the origins of the empirical shapes of force distributions in granular media, emphasizing the role of disorder, local steric constraints, and the influence of anisotropy, with minimal reliance on discrete element method simulations. The models introduced and briefly discussed here support the observed robustness of these force distributions across various systems. Some of the limitations of the present paper will be addressed in a forthcoming paper, where we will present a more detailed comparison with simulation data. In particular, we will investigate the behavior of highly frictional packings, and develop anisotropic joint probability distributions that distinguish explicitly between normal and tangential force components. We will also explore the evolution of force distributions under shear and provide model-based predictions for partial shear stresses. Finally, it is worth noting that exponential force and stress distributions have also been observed in other disordered media, such as porous materials [20]. The vectorial model introduced in this work may serve as a unifying framework in a broad class of disordered macroscopic systems.

References

[1] C. Liu, S.R. Nagel, D.A. Schecter, S.N. Coppersmith, S. Majumdar, O. Narayan, T.A. Witten, Force fluctuations in bead packs, Science **269**, 513 (1995).

[2] D.M. Mueth, H.M. Jaeger, S.R. Nagel, Force distribution in a granular medium, Phys. Rev. E **57**, 3164 (1998).

[3] F. Radjai, M. Jean, J.J. Moreau, S. Roux, Force distributions in dense two-dimensional granular systems, Phys. Rev. Lett. **77**, 274 (1996).

[4] F. Radjai, S. Roux, J.J. Moreau, Contact forces in a granular packing., Chaos **9**, 544 (1999).

[5] F. Radjai, D.E. Wolf, M. Jean, J. Moreau, Bimodal character of stress transmission in granular packings, Phys. Rev. Letter **80**, 61 (1998).

[6] J.H. Snoeijer, T.J.H. Vlugt, M. van Hecke, W. van Saarloos, Force network ensemble: a new approach to static granular matter., Phys Rev Lett **92**, 054302 (2004).

[7] D.H. Nguyen, E. Azéma, F. Radjai, P. Sornay, Effect of size polydispersity versus particle shape in dense granular media, Physical Review E **90**, 012202 (2014).

[8] C. Voivret, F. Radjai, J.Y. Delenne, M.E. Youssoufi, Force transmission in polydisperse granular media, Phys. Rev. Lett. **102**, 178001 (2009).

[9] T.D. Tran, S. Nezamabadi, J.P. Bayle, L. Amarsid, F. Radjai, Contact networks and force transmission in aggregates of hexapod-shaped particles, Soft Matter **20**, 3411 (2024). 10.1039/D3SM01762A

[10] F. Radjai, Modeling force transmission in granular materials, Comptes Rendus Physique **16**, 3 (2015).

[11] L. Rothenburg, R.J. Bathurst, Analytical study of induced anisotropy in idealized granular materials, Geotechnique **39**, 601 (1989).

[12] F. Radjai, J.Y. Delenne, É. Azema, S. Roux, Fabric evolution and accessible geometrical states in granular materials, Granular Matter **14**, 259 (2012).

[13] S.N. Coppersmith, C. Liu, S. Majumdar, O. Narayan, T.A. Witten, Model for force fluctuations in bead packs, Phys. Rev. E **53**, 4673 (1996).

[14] P.T. Metzger, Granular contact force density of states and entropy in a modified edwards ensemble., Phys Rev E Stat Nonlin Soft Matter Phys **70**, 051303 (2004).

[15] R. Youngquist, P. Metzger, K. Kilts, Force density function relationships in 2-d granular media, SIAM J. Appl. Math. **65**, 1855 (2005).

[16] A. Sommerfeld, Thermodynamics and Statistical Mechanics (Academic Press, London, 1955), ISBN 0126546827

[17] N.P. Kruyt, On weak and strong contact force networks in granular materials, International Journal of Solids and Structures **92-93**, 135 (2016). 10.1016/j.ijsolstr.2016.02.039

[18] R. Schoen, Dynamic population models (Springer, 2006)

[19] D.C. Vu, L. Amarsid, J.Y. Delenne, V. Richefeu, F. Radjai, Macro-elasticity of granular materials composed of polyhedral particles, Granular Matter **26**, 6 (2024). 10.1007/s10035-023-01382-3

[20] H. Laubie, F. Radjai, R. Pellenq, F.J. Ulm, Stress transmission and failure in disordered porous media, Phys. Rev. Lett. **119**, 075501 (2017). 10.1103/PhysRevLett.119.075501